# Fluorescence Photoswitching in a Series of Metal-Organic Frameworks Loaded with Different Anthracenes

Min Tu,[a, b] Mariana Lizeth Díaz Ramírez,[c] Ilich A. Ibarra,[c] Johan Hofkens,[d, e] and Rob Ameloot*[a]

The confinement of luminescent guest molecules in porous host materials can induce photophysical properties different from either component in isolation. In this work, we studied several host-guest systems consisting of anthracene and its substituted analogs adsorbed in a series of metal-organic frameworks (MOFs) and inorganic molecular sieves. Fluorescence photoswitching of the guest molecules through photoinduced dimerization is observed only in MOFs with a favorable pore volume and geometry.

## Introduction

Photoswitchable materials undergo reversible changes in their physicochemical properties (*e.g.*, absorbance, fluorescence, electron conductivity) by light irradiation.[1–3] These materials typically contain molecules that switch between two stable forms, such as *trans-* and *cis-*azobenzene,[4] the open and closed form of diarylethenes,[5] or anthracene monomer and photodimer.[6,7] Fluorescence photoswitching of the emission intensity or color in solid-state materials is promising for data storage, anti-counterfeiting, security, and biomedicine.[8–11] Unfortunately, many of the switching characteristics in the solution are not readily transferable to the solid state since the switching mechanism is hindered in a densely packed phase. One promising strategy to overcome this challenge is to confine photoswitchable guests in porous solids, such as zeolites, mesoporous silica, and metal-organic frameworks (MOFs).[12–22]

Crystalline MOFs are nanoporous solids that consist of metal ion nodes connected by multi-topic organic molecules.[23,24] The properties of MOFs, including structural flexibility and tunable pore size, are ideal to confine photoswitchable guests in a variety of nanoenvironments.[14–16] We recently reported reversible solid-state photoswitching of fluorescence through the confinement of anthracene (ANT) in a MOF (zeolitic imidazolate framework 8, ZIF-8).[25] We demonstrated that four ANT molecules organize as two pairs in the cages of ZIF-8, giving rise to excimer emission (maximum at 550 nm, yellow). Upon irradiation of UV light, the limited space in the cage only permits two ANT molecules to photodimerize, resulting in one non-fluorescent ANT photodimer and two non-interacting ANT molecules that emit as monomers (maximum at 415 nm, purple). This phenomenon relies on the match between the ANT guest and the properties of ZIF-8, namely its pore geometry, pore volume, and structural flexibility.[25]

In this work, we encapsulated ANT in several MOFs and inorganic molecular sieves (Figure 1). The differences in pore size, volume, and structural flexibility of the porous host materials resulted in diverse fluorescence properties of these host-guest systems. Moreover, we demonstrated that substituted anthracenes (2-methylanthracene, 2-MA; 9-methylanthracene, 9-MA) in ZIF-8 show similar fluorescence photoswitching behavior as ANT-loaded ZIF-8.

[a] Dr. M. Tu, Prof. R. Ameloot
Centre for Membrane Separations, Adsorption, Catalysis, and Spectroscopy (cMACS)
KU Leuven – University of Leuven
Celestijnenlaan 200F, 3001 Leuven, Belgium
E-mail: rob.ameloot@kuleuven.be
[b] Dr. M. Tu
2020 X-Lab, Shanghai Institute of Microsystem and Information Technology, Chinese Academy of Science Shanghai, Shanghai, 200050, China
[c] M. L. Díaz Ramírez, Prof. I. A. Ibarra
Laboratorio de Fisicoquímica y Reactividad de Superficies (LaFReS),
Instituto de Investigaciones en Materiales,
Universidad Nacional Autónoma de México,
Ciudad de México, Mexico
[d] Prof. J. Hofkens
Department of Molecular Visualization and Photonics,
KU Leuven-University of Leuven,
Celestijnenlaan 200F, 3001 Leuven, Belgium
[e] Prof. J. Hofkens
Max Planck Institute for Polymer Research,
Ackermannweg 10, 55128 Mainz, Germany
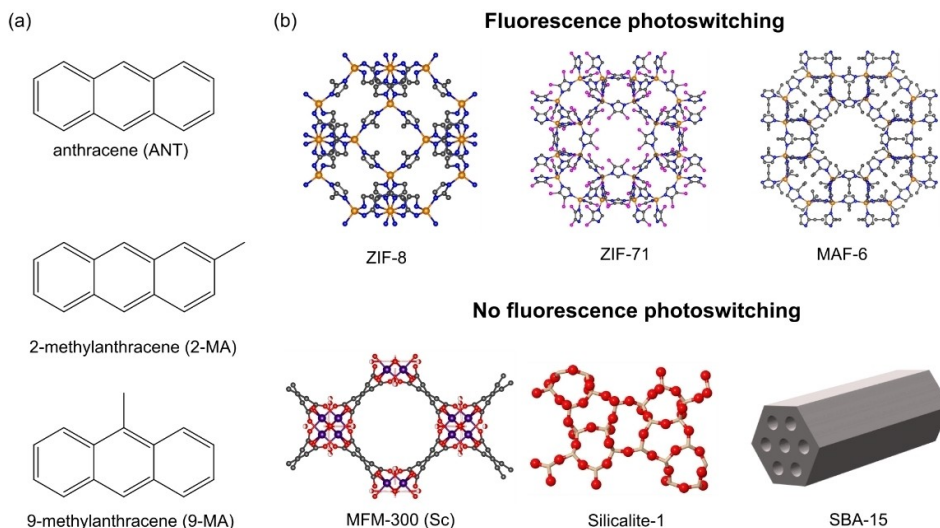Supporting information for this article is available on the WWW under https://doi.org/10.1002/ejic.202100415

## Results and Discussion

The MOFs MAF-6 (metal azolate framework 6) and ZIF-71 consist of $Zn^{2+}$ coordinated by 2-ethylimidazolate (eIm) and 4,5-dichloroimidazolate (dcIm), respectively (Figure 1).[26,27] Both materials crystallize in the zeolitic RHO topology, resulting in truncated cuboctahedral supercages interconnected by octagonal prisms and an effective pore diameter and aperture size of 1.8 and 0.7 nm, respectively.[26,28] For comparison, ZIF-8 has spherical cavities of 1.16 nm in diameter, interconnected by narrow 0.34 nm windows.[25] Although these windows seem too small to permit ANT adsorption, a high loading can be achieved thanks to the framework flexibility.[25] Similarly, ANT can be readily loaded into MAF-6 and ZIF-71 via sublimation. The ANT uptake was determined by thermogravimetric analysis (TGA; Figure 2a). Due to their large pore volume, the maximum ANT loading in MAF-6 and ZIF-71 were 7.2 and 7.4 molecules per

**Figure 1.** Anthracene guests and porous hosts. (a) Chemical structures of ANT, 2-MA, and 9-MA. (b) Ball-stick representation of crystal structures of ZIF-8, ZIF-71, MAF-6, MFM-300 (Sc) and Silicalite-1. All views from b axis. Schematic representation of mesoporous SBA-15. Zn, orange; N, blue; C, grey; Cl, pink; O, red; Sc, purple; Si, brown.
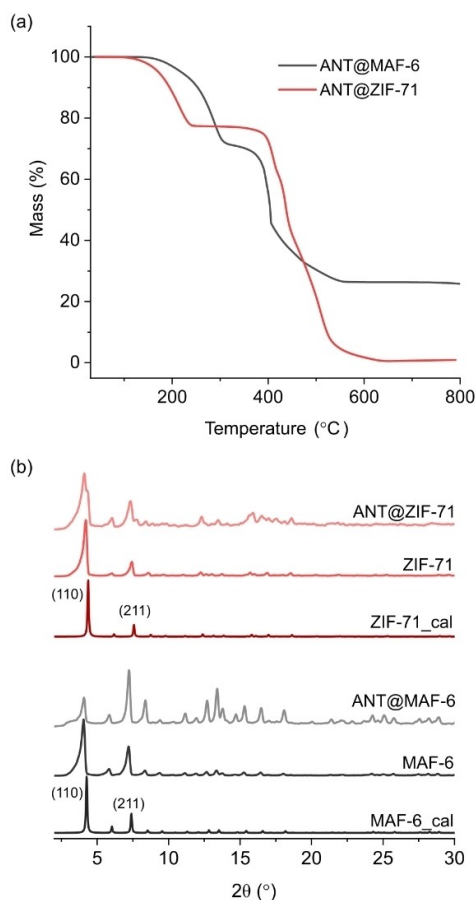


**Figure 2.** Characterization of ANT-loaded MAF-6 and ZIF-71. (a) TGA of ANT-loaded MAF-6 and ZIF-71 in air. The ANT loadings for MAF-6 and ZIF-71 were determined to be 30 wt% and 24 wt%, respectively. (b) PXRD patterns (normalized intensity) of MAF-6 and ZIF-71 before and after ANT loading. The calculated PXRD patterns of the corresponding guest-free MOFs are given for reference.

cage, respectively. These loadings are almost double the maximum loading in ZIF-8 (4 ANT per cage).[25] Powder X-ray diffraction (PXRD) showed that the long-range order is maintained in both MOFs after ANT loading (Figure 2b). The splits of the low-angle reflections of ANT@ZIF-71 indicated a distortion of the unit cell, similar to ANT@ZIF-8.[25] The encapsulation of ANT in MAF-6 and ZIF-71 also resulted in UV-induced fluorescence switching. The emission spectra of ANT@MAF-6 and ANT@ZIF-71 showed broad bands centered at 550 and 500 nm, respectively (Figure 3a, Figure 3c). These emissions are attributed to ANT excimers, whose emission is highly dependent on the arrangement of the two ANT molecules.[29,30] The slightly different pore environments of MAF-6 and ZIF-71 likely result in different ANT organizations and excimer fluorescence. After continuous UV irradiation ($\lambda = 360$ nm), several structured bands appeared for both ANT-loaded MOFs, together with the disappearance of the band at 550 or 500 nm (Figure 3a, Figure 3c), due to ANT photodimerization and remaining monomer emission. *In situ* fluorescence monitoring also revealed the enhancement of the monomer emission (Figure 3b, Figure 3d).

The effect of loading on the fluorescence photoswitching was studied in the ANT@ZIF-71 host-guest system. Different ANT loadings were obtained by varying the ANT:ZIF-71 ratio during sublimation. PXRD patterns of ANT@ZIF-71 showed all the characteristic reflections of ZIF-71 (Figure 4a). With increasing ANT loading, the Brunauer-Emmett-Teller (BET) surface area of the host-guest composites decreased (Figure 4b). At low loadings (<1.5 ANT per cage), monomer emission dominated the emission spectra with only a small broad band centered at 550 nm (Figure 4c). In contrast, broad asymmetric bands appeared for higher loadings, probably because of two different organizations of the ANT pairs and resulting excimer emission bands centered at 430 nm and 550 nm.[31] Furthermore, the ANT
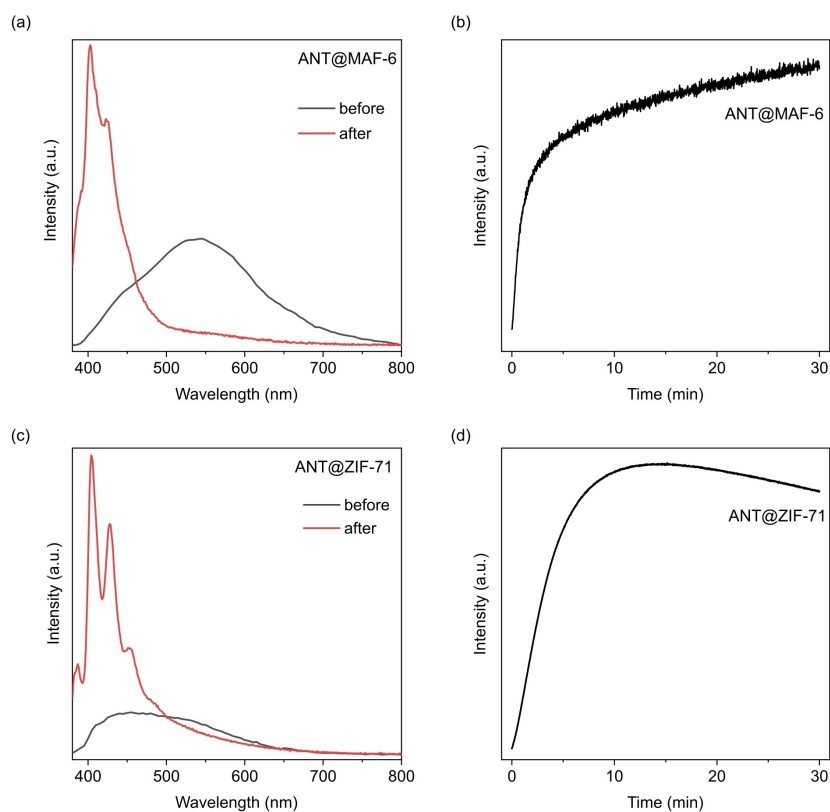
**Figure 3.** Fluorescence photoswitching of ANT-loaded MOFs. Fluorescence emission spectra of ANT@MAF-6 (a) and ANT@ZIF-71 (c) before and after UV irradiation ($\lambda = 360$ nm; 30 min). $\lambda_{ex} = 360$ nm. *In situ* monitoring of the fluorescence emission intensity of ANT@MAF-6 (b; $\lambda_{em} = 415$ nm) and ANT@ZIF-71 (d; $\lambda_{em} = 400$ nm) upon continuous irradiation at $\lambda = 360$ nm.
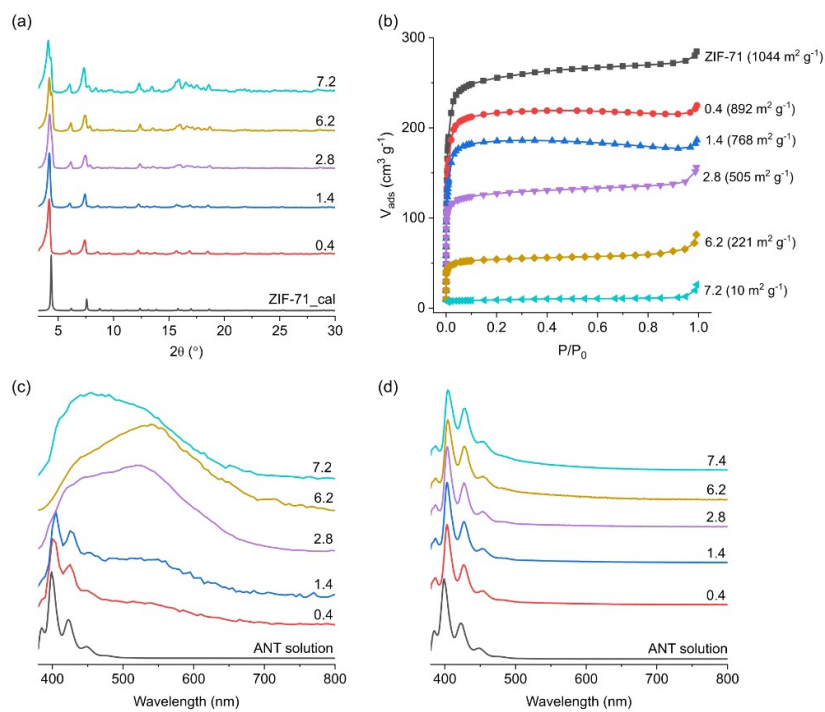


**Figure 4.** Characterization and photoswitching of ANT@ZIF-71 with different guest loadings. (a) PXRD patterns (normalized intensity) of ZIF-71 with different loadings (ANT per cage). The calculated PXRD pattern of ZIF-71 is given for reference. (b) $N_2$ physisorption isotherms (at 77 K) of ANT@ZIF-71 with different loadings and the corresponding BET surface areas. Fluorescence emission spectra (normalized intensity) of ANT@ZIF-71 with different loadings before (c) and after (d) UV irradiation ($\lambda = 360$ nm; 30 min). $\lambda_{ex} = 360$ nm.

monomer emission after UV irradiation is red-shifted for high-loading ANT@ZIF-8 (Figure S6).[25] This phenomenon was attributed to the intermolecular interaction between ANT molecules in neighboring cages. However, UV-irradiated ANT@ZIF-71 exhibited the same fluorescence band ($\lambda_{max}=405$ nm; Figure 4d) irrespective of the ANT loading, probably because the prisms separating the cages prohibited interactions between ANT molecules in neighboring cages.

MFM-300(Sc) crystallizes in the chiral tetragonal space group and shows a binuclear [$Sc_2$(μ-OH)] node, leading to a three-dimensional framework with a pore opening of 0.8 nm (Figure 1b).[28] After the sublimation of ANT into MFM-300(Sc), the relative intensity changes of the PXRD reflections confirm the loading in the pores (Figure 5a), and the TGA data suggested a loading of 1.8 ANT per pore (Figure S7). Similar to
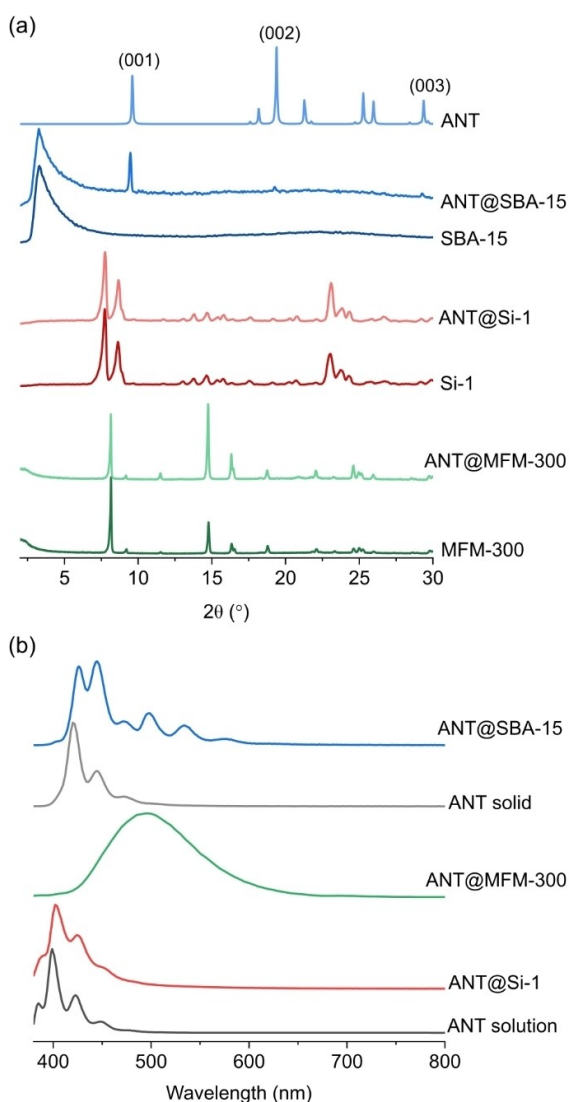


**Figure 5.** Characterization of ANT-loaded MFM-300(Sc), Si-1 and SBA-15. (a) PXRD patterns (normalized intensity) of MFM-300(Sc), Si-1 and SBA-15 with and without ANT loading. PXRD pattern of ANT solid is given for reference. (b) Fluorescence emission spectra of ANT@MFM-300(Sc), ANT@Si-1 and ANT@SBA-15 in comparison with ANT methanol solution (1 mM) and solid. $\lambda_{ex}=360$ nm.

ANT in MAF-6 and ZIF-71, the fluorescence exhibited a broad excimer emission band ($\lambda_{max}=500$ nm; Figure 5b). The two ANT molecules per pore can form an organized pair, giving rise to excimer emission. However, no photoswitching from excimer to monomer emission was observed after UV irradiation (Figure S8).

Similar to MOFs, inorganic molecular sieves such as zeolites and mesoporous silicas also have uniform pore sizes. We studied ANT-loaded molecular sieves with different pore diameters, including Silicalite-1 (Si-1) and SBA-15. Si-1 is a pure-silica zeolite with an MFI topology (Figure 1b). It has straight channels $0.51\times0.55$ nm$^2$ intersecting perpendicularly with sinusoidal channels $0.52\times0.56$ nm$^2$.[33] Due to this narrow channel diameter, the uptake of ANT was hindered, resulting in a low loading by sublimation (2 wt%; Figure S7) and a remaining BET surface area of 277 m$^2$g$^{-1}$ (Figure S9). In contrast, full loading could be achieved in ZIF-8, regardless of its smaller theoretical pore windows, due to the high flexibility of the MOF material. Because of its small pore size and strict confinement, ANT@Si-1 exhibited monomer emission, and no photoswitching was observed (Figure 5b, S8), which is in agreement with results for solution-loaded ANT in ZSM-5 (Na$^+$ form).[33]

SBA-15 has uniform one-dimensional hexagonal mesopores that can be controlled in the range from 4 to 30 nm.[34] Here, 6-nm-pore SBA-15 was employed, which allows high ANT loadings (20 wt%; Figure S7). After ANT loading, several new reflections matching crystalline ANT appeared in the PXRD pattern (Figure 5a),[35] suggesting the crystallization of the guest in the mesopores.[36] The fluorescence spectrum of ANT@SBA-15 was very similar to what would be expected for solid ANT (Figure 5b). In the crystalline state, ANT forms a herringbone arrangement with small π-orbital overlap owing to strong edge-to-face CH-π interactions (Figure S14).[35] Therefore, the ANT solid exhibits the monomer emission, which is slightly red-shifted compared to the monomer emission of a solution in methanol (Figure 5b).[37] Similar to solid ANT, no photoswitching was observed for ANT-loaded SBA-15 (Figure S12).

The substituted ANTs 2-MA and 9-MA can also photo-dimerize upon UV irradiation.[6,7] However, because of their larger size compared to ANT, they could not be loaded effectively into ZIF-8 (Figure S15–16). Therefore, a 'bottle-around-the-ship' encapsulation strategy was used, by having the guest molecule present during the solvent-free crystallization of ZIF-8 (details see Experimental Section).[38] The loadings (0.1–3 molecules per cage) could be controlled through the 2-MA or 9-MA content in the synthesis mixture (Figure S17–18). The PXRD patterns demonstrated the formation of ZIF-8 (Figure 6a, S18) with different loadings. Similar to ANT loading in ZIF-8, the increase of loading gave rise to more intense (200) and (211) reflections.[25]

Monomer emission was observed for low loadings, while excimer emission dominated at high loadings (Figure 6b). Similar to ANT in ZIF-8, UV-induced fluorescence switching of high-loading 9-MA@ZIF-8 from excimer emission to monomer emission was observed (Figure 6b-f). Different from ANT@ZIF-8, the excimer emission diminished but still existed after UV irradiation (Figure 6d). Furthermore, likely due to the intermo-
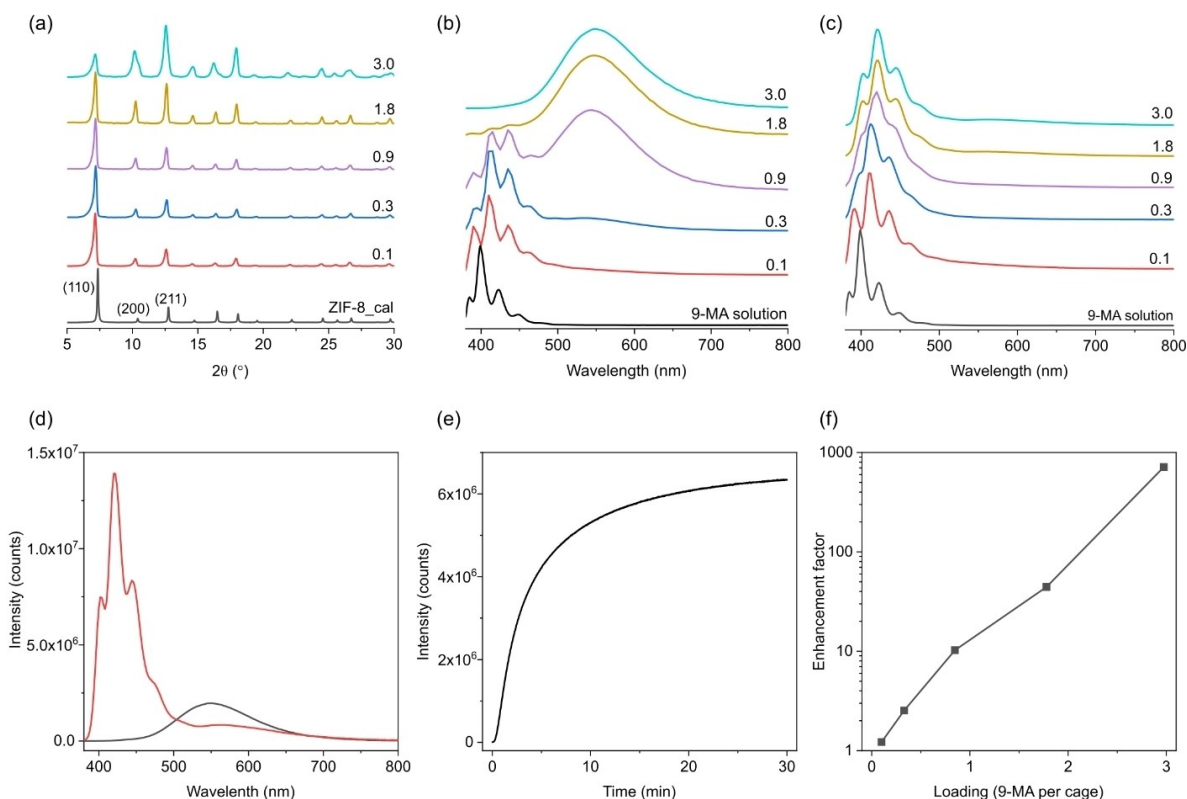
**Figure 6.** Characterization and photoswitching of 9-MA@ZIF-8. (a) PXRD patterns (normalized intensity) of ZIF-8 with different loadings (9-MA per cage). The calculated PXRD pattern of ZIF-8 is given for reference. Fluorescence emission spectra (normalized intensity) of 9-MA@ZIF-8 with different loadings before (b) and after (c) UV irradiation ($\lambda = 360$ nm; 30 min). $\lambda_{ex} = 360$ nm. (d) Fluorescence emission spectra (absolute intensity) of 9-MA@ZIF-8 (3.0) before and after UV irradiation ($\lambda = 360$ nm; 30 min). $\lambda_{ex} = 360$ nm. (e) *In situ* monitoring of the fluorescence emission intensity of 9-MA@ZIF-8 ($\lambda_{em} = 415$ nm) upon continuous excitation at $\lambda = 360$ nm. (f) Fluorescence enhancement of 9-MA@ZIF-8 as a function of the 9-MA loading. The enhancement factor is defined as the ratio of monomer emission intensity ($\lambda = 415$ nm) after and before UV irradiation.

lecular interactions of 9-MA in the neighboring cages, the monomer emission of UV-irradiated 9-MA@ZIF-8 sample was red-shifted at high 9-MA loadings. 2-MA@ZIF-8 also showed similar photoswitching behavior as 9-MA loaded ZIF-8 (Figure S24–26).

## Conclusion

In summary, we studied the photophysical behavior of anthracene and its substituted analogs in different porous materials. Similar to ANT@ZIF-8, fluorescence photoswitching was observed for ANT-loaded MAF-6 and ZIF-71, and 2-MA and 9-MA-loaded ZIF-8. In contrast, no photoswitching was observed for ANT in MFM-300(Sc), Si-1, and SBA-15, due to unsuitable pore sizes and geometries. This work will aid further studies on solid-state photoswitching of host-guest systems based on microporous crystalline materials such as MOFs as hosts.

## Experimental Section

### Materials

All chemicals were purchased from commercial supplies and used without further purification. The abbreviations, supplies, and purities of the chemicals are given below. Pluronic P123 (Sigma-Aldrich), tetraethyl orthosilicate (TEOS, Acros, 98%), zinc oxide (ZnO, 25 nm, Carl Roth, 99%), $Zn(CH_3COO)_2 \cdot 2H_2O$ ($Zn(OAc)_2 \cdot 2H_2O$, Sigma-Aldrich, 98%), 2-methylimidazole (Hmlm, Sigma-Aldrich, 99%), 2-ethylimidazole (Helm, Sigma-Aldrich, 98%), 4, 5-dichloroi-midazole (Hdclm, TCI, 97%), anthracene (ANT, Sigma-Aldrich, 98%), 2-methylanthracene (2-MA, Sigma-Aldrich, 97%), 9-methylanthracene (9-MA, Sigma-Aldrich, 98%), biphenyl-3,3',5,5'-tetracar-boxylic acid ($H_4BTPC$, Sigma-Aldrich), scandium triflate ($Sc(SO_3CF_3)_3$, Sigma-Aldrich, 99%), concentrated HCl (37 wt.%, Sigma-Aldrich), tetrahydrofuran (THF, Sigma-Aldrich, 99%), dimethylformamide (DMF, Sigma-Aldrich, 98%), dichloromethane (DCM, Sigma-Aldrich, 99%), and methanol (MeOH, Sigma-Aldrich, 99%) and Si-1 (Tosoh).

### Synthesis

**MFM-300 (Sc):**[32] 10 mg $H_4BTPC$ and 30 mg $Sc(SO_3CF_3)_3$ were dissolved in a solvent mixture of THF (4.0 mL)), DMF (3.0 mL), deionized $H_2O$ (1.0 mL) and concentrated HCl (100 µL). The mixture was stirred until complete dissolution o and then transferred to a pressure tube. The tube was placed in an oil bath and heated to 348 K for 72 h. After cooling down to room temperature, the

crystalline product was recovered by filtration, washed with DMF (5 mL), acetone-exchanged, and dried in air.

**MAF-6**:[39] A physical mixture of ZnO (162 mg) and 2-ethylimidazole (Helm, 576 mg) was prepared in glass synthesis bottles. The capped bottle was placed in a preheated oven at a temperature of 80 °C for 1 day.

**ZIF-71**:[40] 74 mg Zn(OAc)$_2$·2H$_2$O was dissolved in 15 mL methanol, and 220 mg Hdclm (220 mg) was dissolved in 15 mL methanol. After complete dissolution, the Zn(OAc)$_2$·2H$_2$O solution was poured Hdclm solution. The mixture left standing at room temperature for 1 day.

**ZIF-8**:[41] 68 mg Zn(NO$_3$)$_2$·6H$_2$O was dissolved in 5 mL methanol, and 41 mg HmIm was dissolved in 5 mL methanol. After complete dissolution, the Zn(NO$_3$)$_2$·6H$_2$O in methanol solution was poured into the mIm in methanol solution. The mixture was left standing at room temperature for 1 day.

All the as-synthesized MOF powder samples were collected by centrifugation and washed with methanol by three repetitions of sonication-centrifugation to remove unreacted chemicals. After washing, the ZIF powders were immersed into DCM for 1 day, and subsequently activated at 120 °C under reduced pressure (0.5 mbar) for 6 hours.

**SBA-15**:[42] Pluronic P123 (20 g) was dissolved in deionized H$_2$O (635 g) and concentrated HCl at 35 °C. After a full P123 dissolution, TEOS (43 g) was added for the synthesis of 12 g of silica. This mixture was stirred for 20 h at 35 °C and afterwards filtered and washed. The recovered powder was dried overnight at 80 °C and finally calcined at 550 °C for 6 h (ramp rate: 1 °C min$^{-1}$).

**ANT loading**: To achieve high loading, vials containing a porous material (100 mg) and an excess amount of ANT (300 mg) were placed together in a Schlenk tube. After the evacuation, the Schlenk tube was placed in a preheated oven (120 °C) under a static vacuum (10$^{-1}$ mbar) for 3 days. Afterwards, the samples were collected for different characterizations without further treatment. Different ANT loadings in ZIF-71 (0.4, 1.4, 2.8, 6.2, and 7.2 molecules per cage) were obtained by varying the amount of ANT (5, 10, 25, 50, and 100 mg, respectively).

**2-MA and 9-MA loading in ZIF-8**: The synthesis of 9-MA@ZIF-8 was performed as follows. A mixture of ZnO (162 mg), HmIm (492 mg), and various amounts of 9-MA (10, 30, 60, 100, and 200 mg) was ground in an agate mortar and then transferred into a 10 mL glass vial. Subsequently, the vial was placed into a preheated convection oven at 110 °C for 1 day. Afterwards, the obtained powder sample was washed with methanol (×3 times) to remove the excess HmIm and 9-MA. Finally, the samples were dried at 60 °C in air. The resulted loadings (9-MA per cage) based on this recipe are 0.18, 0.7, 1.42, 2.62, and 3.21. The encapsulation of 2-MA in ZIF-8 was synthesized in a similar fashion.

## Methods

PXRD data were recorded on an STOE COMBI P diffractometer with CuKα1 radiation (λ = 1.54060 Å) and an IP-PSD detector in transmission geometry. Solution $^1$H NMR spectra were recorded on a Bruker Advance 300 MHz spectrometer. The dried ANT, 2-MA and 9-MA-loaded MOF powder (ca. 2 mg) samples were dissolved in a solution containing DCl/D$_2$O (32 wt%, 50 μL) and 500 μL DMSO-d$_6$. TGA was carried out on a Netzsch STA 449F3 instrument with a heating rate of 5 °C min$^{-1}$ under air. The ANT loading (molecule per cage, x) was determined according to the equation [178x/(178x + M$_{pore}$) = mass loss]. The molecular weight of ANT is 178 g mol$^{-1}$. The 'molecular weight' of the pore (M$_{pore}$) of MAF-6, ZIF-71, and MFM-

300(Sc) are 3060, 4044, and 1800 g mol$^{-1}$, respectively, calculated from the crystallographic data (CCDC code: MECWOH, GITVIP, and EXEQAA, respectively). N$_2$ physisorption isotherms were measured at 77 K using a Micromeritics 3Flex instrument. The samples were degassed before measurements at 150 °C under a dynamic vacuum (10$^{-2}$ mbar) for 12 h. The ANT, 2-MA, or 9-MA-loaded samples were degassed at room temperature under dynamic vacuum (10$^{-2}$ mbar) for 12 h. The BET method for all the materials except SBA was applied in the region between 0.005 and 0.05 P/P$_0$, consistent with the consistency criteria for microporous materials.[39] The BET method for SBA and ANT@SBA was applied in the region between 0.1 and 0.3 P/P$_0$. Fluorescence emission spectra were recorded on an FLS 980 fluorescence spectrophotometer (Edinburgh Instruments, Photonics division). The kinetics of the changes in fluorescence emission was recorded *in situ* by monitoring the emission intensity changes upon the excitation light irradiation (λ = 360 nm).

## Conflict of Interest

The authors declare no competing financial interests.

[1] M. Sauer, *PNAS* **2005**, *102*, 9433–9434.
[2] M.-M. Russew, S. Hecht, *Adv. Mater.* **2010**, *22*, 3348–3360.
[3] S. van de Linde, M. Sauer, *Chem. Soc. Rev.* **2014**, *43*, 1076–1087.
[4] C. Zhang, M.-H. Du, H.-P. Cheng, X.-G. Zhang, A. E. Roitberg, J. L. Krause, *Phys. Rev. Lett.* **2004**, *92*, 158301.
[5] M. Irie, T. Fukaminato, K. Matsuda, S. Kobatake, *Chem. Rev.* **2014**, *114*, 12174–12277.
[6] H. Bouas-Laurent, A. Castellan, J.-P. Desvergne, R. Lapouyade, *Chem. Soc. Rev.* **2000**, *29*, 43–55.
[7] H. Bouas-Laurent, A. Castellan, J.-P. Desvergne, R. Lapouyade, *Chem. Soc. Rev.* **2001**, *30*, 248–263.
[8] M. Irie, T. Fukaminato, T. Sasaki, N. Tamai, T. Kawai, *Nature* **2002**, *420*, 759–760.
[9] T. Fukaminato, T. Sasaki, T. Kawai, N. Tamai, M. Irie, *J. Am. Chem. Soc.* **2004**, *126*, 14843–14849.
[10] M. Heilemann, P. Dedecker, J. Hofkens, M. Sauer, *Laser Photonics Rev.* **2009**, *3*, 180–202.
[11] T. Fukaminato, *J. Photochem. Photobiol. C* **2011**, *12*, 177–208.
[12] R. Haldar, L. Heinke, C. Wöll, *Adv. Mater.* **2020**, *32*, 1905227.
[13] A. S. Kumar, T. Ye, T. Takami, B.-C. Yu, A. K. Flatt, J. M. Tour, P. S. Weiss, *Nano Lett.* **2008**, *8*, 1644–1648.

[14] H. A. Schwartz, U. Ruschewitz, L. Heinke, *Photochem. Photobiol. Sci.* **2018**, *17*, 864–873.

[15] B. Gui, Y. Meng, Y. Xie, K. Du, A. C.-H. Sue, C. Wang, *Macromol. Rapid Commun.* **2018**, *39*, 1700388.

[16] A. M. Rice, C. R. Martin, V. A. Galitskiy, A. A. Berseneva, G. A. Leith, N. B. Shustova, *Chem. Rev.* **2020**, *120*, 8790–8813.

[17] G. Tabacchi, *ChemPhysChem* **2018**, *19*, 1249–1297.

[18] K. Weh, M. Noack, K. Hoffmann, K.-P. Schröder, J. Caro, *Microporous Mesoporous Mater.* **2002**, *54*, 15–26.

[19] S. Garg, H. Schwartz, M. Kozlowska, A. B. Kanj, K. Müller, W. Wenzel, U. Ruschewitz, L. Heinke, *Angew. Chem. Int. Ed.* **2019**, *58*, 1193–1197; *Angew. Chem.* **2019**, *131*, 1205–1210.

[20] D. Hermann, H. A. Schwartz, M. Werker, D. Schaniel, U. Ruschewitz, *Chem. Eur. J.* **2019**, *25*, 3606–3616.

[21] Z. Li, G. Wang, Y. Ye, B. Li, H. Li, B. Chen, *Angew. Chem. Int. Ed.* **2019**, *131*, 18193–18199.

[22] Z. Shao, Q. Wu, X. Han, Y. Zhao, Q. Xie, H. Wang, H. Hou, *Chem. Commun.* **2019**, *55*, 10948–10951.

[23] S. R. Batten, N. R. Champness, X.-M. Chen, J. Garcia-Martinez, S. Kitagawa, L. Öhrström, M. O'Keeffe, M. Paik Suh, J. Reedijk, *Pure Appl. Chem.* **2013**, *85*, 1715–1724.

[24] H. Furukawa, K. E. Cordova, M. O'Keeffe, O. M. Yaghi, *Science* **2013**, *341*, 1230444.

[25] M. Tu, H. Reinsch, S. Rodríguez-Hermida, R. Verbeke, T. Stassin, W. Egger, M. Dickmann, B. Dieu, J. Hofkens, I. F. J. Vankelecom, N. Stock, R. Ameloot, *Angew. Chem. Int. Ed.* **2019**, *58*, 2423–2427; *Angew. Chem.* **2019**, *131*, 2445–2449.

[26] X.-C. Huang, Y.-Y. Lin, J.-P. Zhang, X.-M. Chen, *Angew. Chem. Int. Ed.* **2006**, *45*, 1557–1559; *Angew. Chem.* **2006**, *118*, 1587–1589.

[27] R. Banerjee, A. Phan, B. Wang, C. Knobler, H. Furukawa, M. O'Keeffe, O. M. Yaghi, *Science* **2008**, *319*, 939–943.

[28] C.-T. He, L. Jiang, Z.-M. Ye, R. Krishna, Z.-S. Zhong, P.-Q. Liao, J. Xu, G. Ouyang, J.-P. Zhang, X.-M. Chen, *J. Am. Chem. Soc.* **2015**, *137*, 7217–7223.

[29] T. Hinoue, Y. Shigenoi, M. Sugino, Y. Mizobe, I. Hisaki, M. Miyata, N. Tohnai, *Chem. Eur. J.* **2012**, *18*, 4634–4643.

[30] M. Sugino, Y. Araki, K. Hatanaka, I. Hisaki, M. Miyata, N. Tohnai, *Cryst. Growth Des.* **2013**, *13*, 4986–4992.

[31] F. Fennel, J. Gershberg, M. Stolte, F. Würthner, *Phys. Chem. Chem. Phys.* **2018**, *20*, 7612–7620.

[32] I. A. Ibarra, S. Yang, X. Lin, A. J. Blake, P. J. Rizkallah, H. Nowell, D. R. Allan, N. R. Champness, P. Hubberstey, M. Schröder, *Chem. Commun.* **2011**, *47*, 8304–8306.

[33] F. Márquez, H. García, E. Palomares, L. Fernández, A. Corma, *J. Am. Chem. Soc.* **2000**, *122*, 6520–6521.

[34] D. Zhao, J. Feng, Q. Huo, N. Melosh, G. H. Fredrickson, B. F. Chmelka, G. D. Stucky, *Science* **1998**, *279*, 548–552.

[35] J. M. Robertson, W. H. Bragg, *Proc. R. Soc. London Ser. A* **1933**, *140*, 79–98.

[36] L. Yin, D. Wu, Z. Yao, S. Feng, M. Zhang, Y. Gao, *Thermochim. Acta* **2013**, *565*, 72–81.

[37] B. Stevens, *Spectrochim. Acta* **1962**, *18*, 439–448.

[38] I. Stassen, M. Styles, G. Grenci, H. V. Gorp, W. Vanderlinden, S. D. Feyter, P. Falcaro, D. D. Vos, P. Vereecken, R. Ameloot, *Nat. Mater.* **2016**, *15*, 304–310.

[39] T. Stassin, I. Stassen, J. Marreiros, A. J. Cruz, R. Verbeke, M. Tu, H. Reinsch, M. Dickmann, W. Egger, I. F. J. Vankelecom, D. E. De Vos, R. Ameloot, *Chem. Mater.* **2020**, *32*, 1784–1793.

[40] R. P. Lively, M. E. Dose, J. A. Thompson, B. A. McCool, R. R. Chance, W. J. Koros, *Chem. Commun.* **2011**, *47*, 8667–8669.

[41] J. Cravillon, S. Münzer, S.-J. Lohmeier, A. Feldhoff, K. Huber, M. Wiebcke, *Chem. Mater.* **2009**, *21*, 1410–1412.

[42] R. Locus, D. Verboekend, M. d'Halluin, M. Dusselier, Y. Liao, N. Nuttens, T. Jaumann, S. Oswald, L. Mafra, L. Giebeler, B. Sels, *ChemCatChem* **2018**, *10*, 1385–1397.

[43] K. S. Walton, R. Q. Snurr, *J. Am. Chem. Soc.* **2007**, *129*, 8552–8556.